THE JOURNAL OF PHYSICAL CHEMISTRY C

Article

pubs.acs.org/JPCC

Surface Behavior of Aprotic Mixtures: Dimethyl Sulfoxide/Acetonitrile

Javier Rodriguez,[†,‡] M. Dolores Elola,[†] Jordi Martí,[§] and Daniel Laria*[,†,∥]

[†]Departamento de Física de la Materia Condensada, Comisión Nacional de Energía Atómica, Avenida Libertador 8250, 1429 Buenos Aires, Argentina

[‡]ECyT, UNSAM, Martín de Irigoyen 3100, 1650 San Martín, Pcia. de Buenos Aires, Argentina

[§]Department of Physics, Technical University of Catalonia, Barcelona Tech. B5-209 UPC Northern Campus, Jordi Girona 1-3, 08034 Barcelona, Catalonia, Spain

[∥]Departamento de Química Inorgánica, Analítica y Química-Física and INQUIMAE-CONICET, Facultad de Ciencias Exactas y Naturales. Universidad de Buenos Aires Ciudad Universitaria, Pabellón II, 1428 Buenos Aires, Argentina

ABSTRACT: We present results from molecular dynamics simulations that examine microscopic characteristics of mixtures combining acetonitrile (ACN) and dimethyl sulfoxide (DMSO) at the vicinity of liquid/air and liquid/graphene interfaces. In the former interfaces, our simulations reveal a clear propensity of ACN to lie adjacent to the vapor phase at all concentrations. A simple model based on the consideration of a chemical equilibrium between bulk and surface states was found to be adequate to reproduce simulation results. Orientational correlations at the interface showed a mild tendency for dipolar aligments pointing toward the vapor phase in ACN-rich solutions; contrasting, in DMSO-rich mixtures, the preferential orientations looked mostly parallel to the interface. Close to graphene plates, the local scenarios reverse and local concentrations of DMSO are larger than the one observed in the bulk. Dynamical results reveal that the characteristic time scales describing orientational relaxations and residence times at the interfaces stretch as the concentration of ACN diminishes. For liquid/air interfaces residence times for ACN were found to be larger than those for DMSO. A classical treatment for the predictions of the C−H stretching band of the IR peaks in the bulk and at the interfaces reveals shifts that agree with experimental measurements.

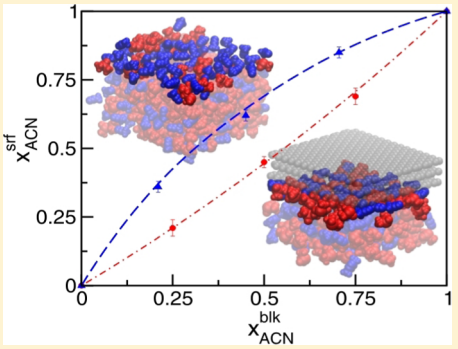

I. INTRODUCTION

Acetonitrile (ACN) and dimethyl sulfoxide (DMSO) represent prototypical examples of aprotic polar solvents with practical applications in areas as diverse as cryoprotection,[1] liquid chromatography,[2] energy storage devices,[3] medicinal chemistry,[4] and atmospheric sciences,[5] to cite a few relevant examples. On the basis of their common aprotic character and the similarities between their corresponding dipole moments, 3.96 D (ACN) versus 3.92 D (DMSO) and dielectric constants (both close to ∼40), one would be tempted to conclude that chemical reactivity in these two media should not differ in a substantial fashion. However, in fact, the latter statement is only partially true. For example, the experimentally reported dissociation constant of HCl in DMSO is practically 6 orders of magnitude larger than the one observed in ACN.[6,7] Computer simulations have demonstrated that these differences can be ascribed to modifications in the ionic solvation structures, which lead to much more stable solvent-separated ion pairs in DMSO.[8] Clearly, the physical interpretations of these subtleties require much more detailed analyses that go beyond the simple consideration of the dipole moments or the collective polarization responses of the two species.

Mixtures combining these two solvents open possibilities for "intermediate" solvation environments between the limiting, pure liquid, structures. However, in many cases, the resulting scenarios deviate considerably from the ideal-mixture behaviors. In a recent paper, we reported a molecular dynamics analysis of solvation of simple ionic species in these mixtures that showed a marked asymmetry in the solvation of Li^+-Cl^- ion pairs, with a clear preference of DMSO for cationic solvation at practically all concentrations.[9] These differences, in turn, were also registered in conductivity results that showed pronounced changes in ionic mobilities in ACN-rich solutions with concentrations as high as $x_{ACN} \sim 0.95$.[10] All these nonidealities contrast sharply with the results reported by Bernardi et al.[11] for the internal energies of the mixtures which show only mild positive deviations, and with the experimental molar volumes, which follow a linear dependence with the individual concentrations.[12]

Microscopic descriptions of these mixtures in the vicinity of interfaces incorporate additional ingredients to these, already complex, bulk solvation structures; most notably are those

Received: April 3, 2017
Revised: June 21, 2017
Published: June 21, 2017

DOI: 10.1021/acs.jpcc.7b03154
J. Phys. Chem. C 2017, 121, 14618−14627

related to the strong gradients in the intermolecular forces that prevail in these environments. The behavior of mixtures involving polar aprotic solvents at liquid/vapor and liquid/solid interfaces has received considerable attention in recent years; however, these studies have focused on combinations involving, almost exclusively, water (W) as cosolvent.[13−23] The specific case of ACN−W mixtures is particularly enlightening since many characteristics of the prevailing structures of the liquid mixtures could be rationalized invoking the well-documented hydrophobicity of the water/air interface,[24−26] contraposed with the hydrophilic character of hydroxylated silica surfaces. The latter characteristics clearly control the gross features of concentration fluctuations at the interfaces which, in some cases, may even lead to structures compatible with microscopic demixing phenomena.[13,19,27] Unfortunately, similar interpretations performed on mixtures of aprotic solvents at interfaces have a much more limited scope.

These limitations underline the main motivation of the present work, in which we examine microscopic characteristics of ACN/DMSO mixtures at liquid/air and liquid/graphene interfaces, using molecular dynamics techniques. Our study includes a detailed analysis of concentration fluctuations at the different interfaces along with the corresponding orientational correlations. For the particular case of graphene, we have explored the modifications operated at the interfaces by the addition of Coulomb coupling between the liquid phase and the walls to gain insights about solvation structures of these mixtures at the vicinity of charged electrodes. This information might have potential relevance in the design of lithium-ion batteries.[28] On the dynamical side, we focused attention on two relevant dynamical modes. The first one corresponded to diffusive motions perpendicular to the interfaces, interpreted by the corresponding residence times. In addition, we also investigated relaxations of orientational motions. The paper concludes with a classical analysis of the characteristics of the shifts operated in the C−H stretching bands of the corresponding IR spectra at the surfaces by comparing them with those obtained from simulations in the bulk.

The organization of the paper is as follows: Details of the model and technical details of the simulations are provided in section II. Sections III and IV include results for equilibrium and dynamical properties, respectively. In section V, we summarize the main conclusions of the work.

II. MODELS AND TECHNICAL DETAILS OF THE SIMULATIONS

Liquid/Air Interfaces. Computer simulations were performed on ACN/DMSO mixtures, with global concentrations x_{ACN} = 0.25, 0.5, and 0.75. As references, a few test runs were also undertaken for pure liquid phases. Our procedure started by performing equilibration runs on fully periodic, bulk phases, at T = 298 K. The lengths of the original rectangular cells were fixed at $L_x = L_y$ = 40 Å and L_z = 50 Å, whereas the numbers of molecules of each species, N_α (α = ACN, DMSO), were adjusted so as as to bring the densities of the mixtures in agreement with the experimental results reported in ref 12. Following these initial stages, we enlarged L_z up to 150 Å and performed additional canonical runs for about ∼100−200 ps, using a Nosé−Hoover thermostat.[29,30] With this procedure, we obtained stable liquid/vapor interfaces showing practically no evaporation episodes.

All molecules were modeled as fully flexible collections of atoms. For DMSO, we adopted the *FS* potential reported in ref 31, whereas for ACN, we implemented the *C* model developed by Nikitin et al.[32] To evaluate cross-interactions, we resorted to the classical arithmetic and geometric means for length and energy parameters describing Lennard-Jones, dispersive interactions. This combination of force fields provided liquid mixtures showing no meaningful modifications in pair correlation functions and no evidence of phase separation artifacts along time spans of the order of a few tens of nanoseconds.

Short-range intermolecular forces were computed using a cutoff distance of 13 Å, while the long nature of the electrostatic forces was treated by implementing Ewald sums, using a particle mesh method. Appropriate sampling of equilibrium properties required of the order of ∼3−5, statistically independent, canonical runs, lasting typically ∼20 ns each. On the other hand, dynamical properties were computed from microcanonical runs of similar duration. All simulations were performed using the NAMD package.[33]

Liquid/Graphene Interfaces. Mixtures confined within graphene walls were prepared following a protocol similar to the one described previously. In this case, the mixtures were confined within two graphene plates, held fixed at $z = \pm 40$ Å, with planar surfaces perpendicular to the z-axis. The plates consisted of three rigid atomic layers containing 448 atoms each, with closest interatomic distances set at 1.42 Å. The linear dimensions of the sheets were 34.08 Å × 34.43 Å. As a distinctive feature, at each value of x_{ACN}, we started by performing a series of simulation runs in which, by trial and error, the numbers of molecules of each species were fixed so as to bring the local densities at the $z \sim 0$, "bulk" region, in agreement with the corresponding experimental values. In doing so, we found local molar fractions x_{ACN}^{blk} that deviated at most in 1−2% from the preset x_{ACN} values. Two kinds of simulation experiments, differing in the characteristics of liquid/plates interactions, were undertaken: In the first one, solvent−graphene interactions were considered exclusively of the Lennard-Jones type. The parametrization of the energy and length parameters for C atoms in the plates was taken from the CHARMM27 library:[34] σ_C = 3.55 Å and ϵ_C = 0.07 kcal mol^{-1}. In order to explore the modifications observed in the liquid mixtures in the vicinity of charged electrodes, we also performed a second set of simulations in which total charges $Q = \pm 4.48$ e were uniformly distributed across the atomic positions of the layers directly exposed to the mixtures, giving rise to global charge densities of $\sigma_q \sim \pm 6.1$ μC cm^{-2}. Recent studies[35] have demonstrated limitations in descriptions based on uniform charge distributions, in contraposition with more realistic ones that impose the correct electrostatic, constant voltage, boundary conditions.[36] Anyhow, subsequent analyses[37] have shown that these inadequacies become relevant for charge densities greater than the one investigated here.

III. EQUILIBRIUM RESULTS

Liquid/Air Interfaces. The starting point of our analysis will be the examination of local density fluctuations associated with the two species in the vicinity of the liquid/air interfaces. In particular, we will focus attention on $g_\alpha(z)$, namely

$$g_\alpha(z) = \frac{1}{\rho_\alpha^{blk} L_x L_y} \sum_{i=1}^{N_\alpha} \langle \delta(Z_i^\alpha - Z_{CM} - z) \rangle \quad (1)$$

where $\langle ... \rangle$ denotes an equilibrium ensemble average; in addition, Z_i^α and Z_{CM} correspond to the z-coordinates of the

DOI: 10.1021/acs.jpcc.7b03154
J. Phys. Chem. C 2017, 121, 14618−14627

center of mass of the ith molecule of species α in the mixture and the center of mass of the slab, respectively. In the same expression, ρ_α^{blk} represents the bulk density of component α; the latter values were adjusted so that all g_α plots level off at unity for $z \sim 0$. In what follows, we will show that due to the characteristics of the local concentration fluctuations at the interfaces, the values of ρ_{ACN}^{blk} were found to be somewhat smaller than those estimated from the global stoichiometry of the mixtures (see entries listed in column 2 of Table 1). These differences are due to finite size effects that scale as $V^{-1/3}$ and, consequently, should progressively disappear in larger systems.

Table 1. Local Concentrations of ACN/DMSO Mixtures in the Vicinity of Different Interfaces

x_{ACN}	x_{ACN}^{blk}	x_{ACN}^{srf}	$x_{ACN}^{srf}/x_{ACN}^{blk}$	$\bar{A}$ (Å^2)
a. liquid/air interfaces				
0.0	0.0	0.00		25.3
0.25	0.21	0.36	1.7	23.5
0.50	0.45	0.63	1.4	22.3
0.75	0.71	0.85	1.2	21.5
1.0	1.00	1.00	1.0	20.8
b. liquid/graphene interfaces				
0.25	0.25	0.21	0.84	25.4
0.50	0.50	0.45	0.90	23.4
0.75	0.75	0.69	0.92	22.6

Results for $g_\alpha(z)$ for different mixtures are depicted in Figure 1; as references, we have also included results for liquid/air interfaces of pure-solvent slabs. As we move from the vapor toward the liquid phase, DMSO plots present gradual increments in agreement with the usual "hyperbolic-tangent profiles", with widths that become wider as x_{DMSO} diminishes. Contrasting, the ACN profiles look shifted toward the vapor phase and exhibit net enhancements of the local densities at the interface compared to the bulk values. These increments become more marked as the global concentration of ACN diminishes, reaching $g_{ACN}(z = 23\ Å) \sim 1.8$ for the $x_{ACN} = 0.25$ mixture.

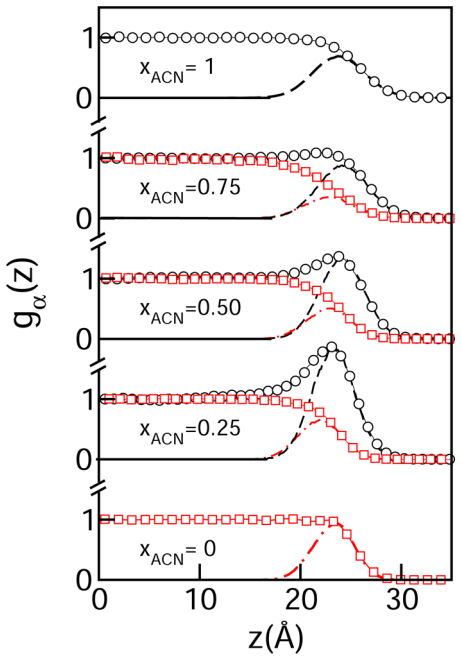

Figure 1. Local densities of ACN (open circles) and DMSO (open squares) for different mixtures at the liquid/air interfaces. Also shown are results for densities of molecules lying at the interface. ACN (dashed black lines) and DMSO (dash-dotted red lines).

The profiles depicted in Figure 1 represent thermally averaged results that do not allow for a clear identification of the modifications operated in the number and in the identity of the tagged molecules lying at the instantaneous interfaces. Different methods, mostly based on geometrical considerations, have been devised to keep track of interfacial molecules.[18,38−42] For the present case, we found it practical to resort to a strategy based on probe particles,[22,23,43,44] which can be implemented in multicomponent systems in a straightforward fashion. Briefly, the algorithm involves approaching a test sphere along the z-direction, from the vapor toward the liquid phases, keeping its x and y coordinates fixed at a series of grid points spanning the $x-y$ plane. The approach is interrupted once the distance between the test sphere and a tagged site in the liquid phase attains a low-threshold value. With this procedure, a molecule was considered as lying at the interface if at least one of its atomic sites was intercepted by the test sphere. In the present case, the grid comprised a total of equally spaced, 40 × 40 points, whereas the threshold distances of encounter were computed from arithmetic means involving the Lennard-Jones length parameters of the tagged sites and the diameter of the test sphere that was set to 4 Å. The interested reader is referred to ref 43 for a comprehensive discussion about appropriate choices of these parameters.

Local densities corresponding ACN and DMSO surface molecules, normalized in a similar fashion to the one implemented in the computation of the $g_\alpha(z)$ profiles, appear in Figure 1 with black-dashed and with red-dotted-dashed lines, respectively. In all cases, the plots look reasonably Gaussian-like, with widths of the order of ∼2 Å. ACN distributions look ∼1 Å shifted toward the vapor phase, compared to the DMSO counterparts, and are centered at positions that practically coincide with those of the maxima of the $g_{ACN}(z)$ (open circles). DMSO density curves are centered close to the corresponding Gibbs dividing surfaces, computed invoking the usual midpoint criterion between the 90%−10% liquid bulk densities.

The integrals over the Gaussian profiles provide estimates for the local compositions at the slab surfaces x_α^{srf}. In Figure 2, we present results for surface versus bulk compositions. Typically,

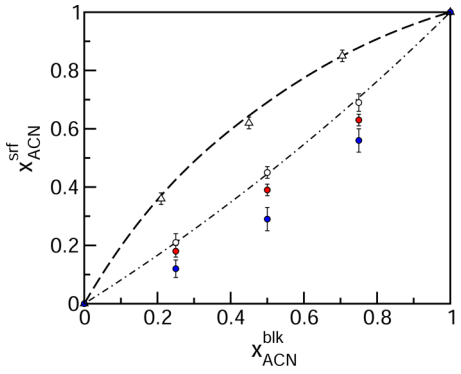

Figure 2. Surface local concentrations for different mixtures: liquid/air interfaces (triangles); liquid/graphene interfaces ($Q = 0$: open circles; $Q > 0$: red circles; $Q < 0$: blue circles). The dashed and dot-dashed lines correspond to predictions from eq 2 (see text).

DOI: 10.1021/acs.jpcc.7b03154
J. Phys. Chem. C 2017, 121, 14618−14627

these interfaces can accommodate a total of 65−75 molecules, yielding results for the area per molecule of the order of $\bar{A} \sim 23$ Å^2 (see values listed in columns 6 of Table 1). Similar estimates have been reported for DMSO interface in Table 2 of ref 18. The plot shown in Figure 2 (triangles) reveals clear enhancements of the local concentration of ACN at the surface, attaining a value ∼70% larger than the one observed in the bulk for the $x_{ACN} = 0.25$ mixture (see column 4 of Table 1).

The observed propensity of ACN to lie at the surface can be further rationalized invoking a simple model in which the surface layer and the adjacent bulk environment are considered as two phases in equilibrium. By establishing that the chemical potential of each species at the bulk and at surface are equal, a straightforward mathematical treatment leads to the following approximate expression:[45,46]

$$x_{ACN}^{srf} \sim \frac{x_{ACN}^{blk}}{\omega(1 - x_{ACN}^{blk}) + x_{ACN}^{blk}} \quad (2)$$

with

$$\omega = \exp\left[\frac{(\gamma_{ACN}^{lv} - \gamma_{DMSO}^{lv})\bar{A}}{k_B T}\right] \quad (3)$$

In the previous expression, γ_α^{lv} represents the liquid/vapor surface tension of the pure component α and $\bar{A}$ denotes the mean surface area per molecule in the mixture. Two basic approximations are involved in the derivation of eq 2: (i) The first one establishes that the ratio between the activity coefficients of each component in the bulk and at the surface are similar, so that the ratio of activities can be approximated by the ratio of the corresponding molar fractions, namely

$$a_\alpha^{srf}/a_\alpha^{blk} \sim x_\alpha^{srf}/x_\alpha^{blk} \quad (4)$$

(ii) The second one considers that the areas per molecule of each species are also comparable, i.e., $\bar{A}_{DMSO} \sim \bar{A}_{ACN} \sim \bar{A}$ which, in the present case, holds within ∼5% differences. Note that according to eq 2, the ACN preference to lie at surface is controlled by the ω term, i.e., the Boltzmann factor involving the difference between the surface tensions of the two components; this underlies the well-known physical interpretation of γ_α^{lv} in terms of the reversible work per unit of area required to bring α-molecules from the bulk to the surface. Results for x_{ACN}^{srf} obtained from eq 2 are also shown in Figure 2 (dashed line). They were computed using the experimental values of $\gamma_{ACN}^{lv} = 28.5$ erg cm^{-2} and $\gamma_{DMSO}^{lv} = 42.8$ erg cm^{-2} at $T = 298$ K reported in ref 47 and assuming a single value of $\bar{A} = 23$ Å^2. Given the simplicity of the arguments involved in the derivation of the approximate eq 2, the degree of agreement is remarkable, although we cannot discard that it might also be partially fortuitous.

We will now move to the examination of local polarization fluctuations in the vicinity of the free interfaces. The most direct route to gain insight about these fluctuations involves the computation of distribution functions of the type

$$P_\mu^\alpha(\cos\theta) = \frac{1}{N_\alpha^{srf}} \sum_{i=1}^{N_\alpha^{srf}} \langle \delta(\cos\theta_i - \cos\theta)\rangle_{srf} \quad (5)$$

with

$$\cos\theta_i = \frac{\boldsymbol{\mu}_i^\alpha \cdot \hat{\mathbf{z}}}{|\boldsymbol{\mu}_i^\alpha|} \quad (6)$$

In the previous equations, $\boldsymbol{\mu}_i^\alpha$ represents the dipole moment of the ith molecule of species α; $\hat{\mathbf{z}}$, a unit vector along the z-direction, and $\langle\cdots\rangle_{srf}$ denotes a sampling restricted to the N_α^{sfr} molecules lying at the interface. Results for $P_\mu^{ACN}(\cos\theta)$ appear in the top panel of Figure 3. All distributions show broad

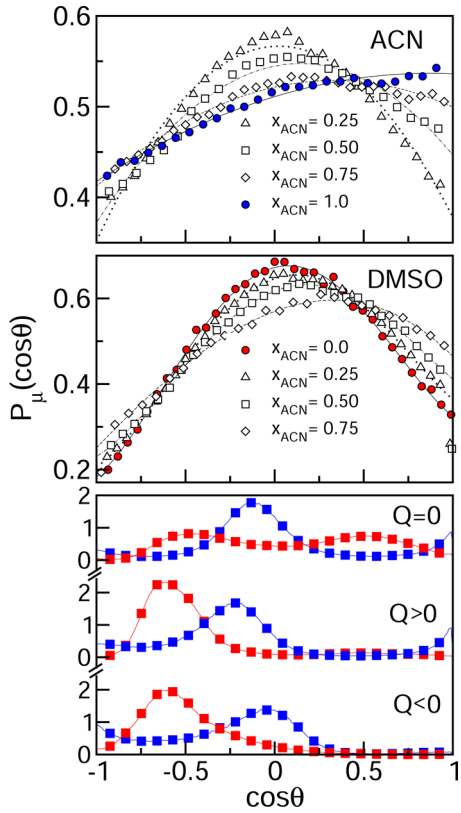

Figure 3. Polarization distributions at different interfaces. Top and middle panels contain results for ACN and DMSO for liquid-mixture/air interfaces. Bottom panel: distribution for dipolar orientations at liquid/graphene interfaces for an $x_{ACN} = 0.5$ mixture. Red and blue squares correspond to results for DMSO and ACN, respectively.

profiles, with a mild tendency favoring dipolar orientations pointing out, toward the gas phases. This tendency is less marked as the concentration of ACN decreases; note that for the $x_{ACN} = 0.25$ case, the dipolar distribution looks practically symmetric with respect to $\cos\theta = 0$. In passing, we would like to comment on some differences between the $x_{ACN} = 1$ results presented here and those shown in Figure 2 of ref 48 and in Figure 5b of ref 49. These discrepancies can be ascribed to the fact that in the latter cases the samplings were restricted to external layers with widths comparable to the size of the ACN molecule; under these circumstances "overcounted" dipoles from molecules lying at adjacent regions may introduce apparent discrepancies in distributions obtained with different atomic locations.[49] Distributions for surface polarization for DMSO are shown in the middle panel of Figure 3. At a qualitative level, the curves do not differ substantially from the ones observed for ACN, with a polarization-versus-concentration trend similar to the one observed in the top panel. Note that results for the limiting $x_{ACN} = 0$ case agree to results reported in refs 44 and 50, indicating that the O═S bond remains parallel to the surface.

Liquid/Graphene Interfaces. We will now move to the analysis of liquid/graphene interfaces, examining local site

DOI: 10.1021/acs.jpcc.7b03154
J. Phys. Chem. C 2017, 121, 14618−14627

densities in the vicinity of uncharged plates which are depicted in the top panel of Figure 4. The plots correspond distribution

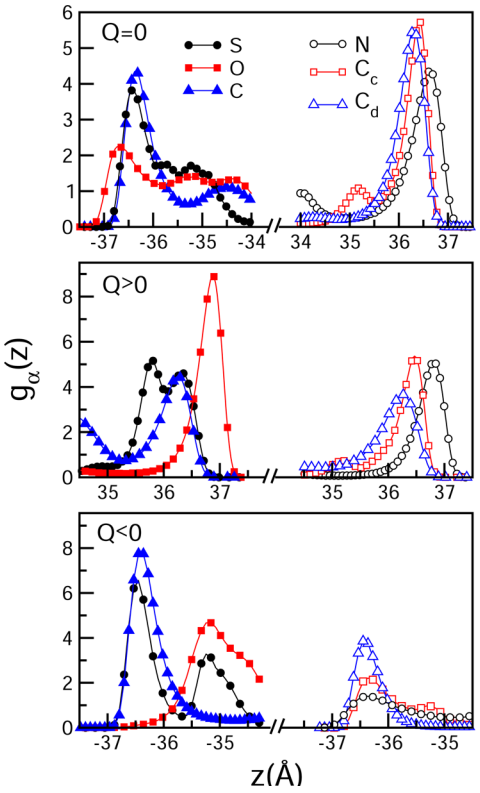

Figure 4. Local site densities of ACN (open symbols) and DMSO (filled symbols) for an x_{ACN} = 0.5 mixtures in the vicinity of different liquid/graphene interfaces. Top panel: uncharged plate; middle panel: positively charged plate; bottom panel: negatively charged plate. Filled (open) symbols correspond to DMSO (ACN) molecules. C_d and C_c denote distal and central atoms in the ACN molecule, respectively (see text).

functions similar to the ones described in eq 1 for the z-components of different site coordinates. For the sake of concision, we will restrict our analysis to the x_{ACN} = 0.5 case as a representative mixture, unless necessary to illustrate distinctive features. The plots present highly irregular characteristics that extend for about ∼10−15 Å inward from the plates before level off at unity. To facilitate the description, it will be instructive to simultaneously analyze the results of the distribution of local polarizations that appear in the bottom panel of Figure 3 (Q = 0). In this case, the sampling was restricted to those molecules with at least one site lying under the main peaks of $g_\alpha(z)$, i.e., those satisfying $|z_\alpha^i| > 35.5$ Å. For ACN, the polarization distribution (blue squares) exhibits a broad main peak at $\cos\theta \sim -0.15$ and a much milder feature at $\cos\theta \sim 1$. As such, molecular configurations in which the ACN axis lies practically parallel to the solid surface prevail, along with a smaller probability of arrangements in which only the positively charged, distal CH_3 with dangling H remains in contact with the solid substrate. The set of curves in Figure 4 confirms this geometrical arrangement: Note that the main peaks for the three axial sites lie within an ∼0.5 Å wide interval, centered at ∼36.4 Å, and exhibiting comparable areas; in addition, one can also perceive secondary peaks ∼1.3 Å (C-central) and ∼2.4 Å (N) inward into liquid phase; these lengths are comparable to the intramolecular distances between the C-distal and the latter sites, indicating molecular orientations mostly perpendicular to the graphene sheet. The $g_\alpha(z)$ profiles for DMSO look more irregular, which is somehow expected given the larger variety of intramolecular length scales controlling the resulting molecular packing at the graphene walls. The interpretation of the dipolar distribution (red squares) with a bimodal character looks much more straightforward, suggesting that configurations with the CH_3 groups and O-sites in contact with the plates are equally likely to be observed.

Local concentrations of the two species at the graphene walls are listed in column 3 of Table 1b and are also depicted in Figure 2 (open circles). Contrasting with the liquid/air interfaces, the observed propensity is reversed and the local concentrations of ACN at the walls are smaller than those prevailing in the bulk phases. In addition, the magnitudes of these modifications look less marked compared to the ones reported for liquid/air interfaces. We further exploited the simplicity of the different hypothesis leading to eq 2 to analyze this qualitative modification in the trends. Equation 2 requires estimates for the difference between liquid/solid surface tensions, $\gamma^{ls}_{ACN} - \gamma^{ls}_{DMSO}$, which, in turn, can be obtained via the classical Young expression, namely

$$\gamma^{ls}_{ACN} - \gamma^{ls}_{DMSO} = \gamma^{lv}_{DMSO}\cos\theta^{Y}_{DMSO} - \gamma^{lv}_{ACN}\cos\theta^{Y}_{ACN} \qquad (7)$$

where θ^Y_α represents the contact angle at the liquid/gas/solid intersection. Unfortunately, we failed to find direct experimental data for these angles; as an alternative, we resorted to the correlation reported by Shen et al.[51] between $\cos\theta^Y_\alpha$ and the so-called "dispersive" and "polar" components[52,53] of γ^{lv}_α for a series solvents, including DMSO and ACN.[54] Results from eqs 2 and 7, with $\cos\theta^Y_\alpha$ set at 0.70 (DMSO) and 0.92 (ACN) and $\bar{A}$ = 24 Å^2, appear in Figure 2 (dot-dashed lines).[54] Similarly to what we registered for the liquid/vapor interfaces, eq 2 appears equally successful in capturing the basic ingredients controlling concentration fluctuations in the vicinity of the graphene walls as well. In passing, we remark the reported disparity[51] between the "dispersive/polar" ratios for the ACN = 0.45 and for DMSO = 4.5 which, in turn, would suggest that the inversion in the surface propensity could be ascribed mostly to a stronger nature of the surface unbalances in the dispersive DMSO−graphene interactions.

Compared with the previous Q = 0 cases, the incorporation of additional Coulomb coupling between the plates and the liquid mixtures promotes more marked deviations in the local densities from the bulk ones (see colored circles in Figure 3). For example, for the x_{ACN} = 0.5 mixture, the ACN depletions at charged interfaces fall down to x^{srf}_{ACN} = 0.38 ± 0.03 for the $Q > 0$ plate (cathode) and x^{srf}_{ACN} = 0.29 ± 0.03 for the $Q < 0$ plate (anode). Note that these asymmetries in the solvation at the walls could not be anticipated based on the sole consideration of the magnitudes of the corresponding dipolar moments, which for ACN and DMSO are of similar magnitude. This reinforces the idea that the prevailing local structures are the result of complex interplays between packing effects and Coulomb couplings of difficult prediction. Still, as expected, the plots for $g_\alpha(z)$ at the anode (middle panel of Figure 4) are dominated by main peaks for negatively charged sites, located at $z \sim 37$ Å, whereas the mirrored scenario appears at the cathode, where the main peak at $z \sim -36.5$ Å now corresponds to the methyl carbons (bottom panel). Polarization distributions shown in the bottom panel of Figure 3 ($Q \neq 0$) exhibit

DOI: 10.1021/acs.jpcc.7b03154
J. Phys. Chem. C 2017, 121, 14618−14627

shifts toward negative values of cos θ (somewhat more marked for the DMSO molecules); this observation is accordant with the presence of a net polarization, parallel to the external electric field spanning the fluid phase.

IV. DYNAMICAL CHARACTERISTICS

We will begin our dynamical analysis by focusing on the characteristics of translational and rotational motions of the two components at the different interfaces. One should keep in mind that the presence of the different interfaces brings the different dynamical modes anisotropic. Exploiting the cylindrical symmetry of the systems, parallel and perpendicular diffusion coefficients are normally computed from restricted samplings of mean-square displacements in the vicinity of interfaces[55−58] or from a more complex computation of the diffusion tensor at the interfaces.[59] Information about the perpendicular diffusive characteristics of interfacial molecules can be extracted from the values of τ^{res}, the average residence times. As such, one should reasonably expect that larger diffusion constants along the latter axis should go hand-in-hand with shorter residence times and vice versa.

The usual route to estimate τ_{res} involves the computation of time correlation functions of the type

$$C_\alpha^{res}(t) = \frac{\langle \eta_\alpha^i(t)\cdot\eta_\alpha^i(0)\rangle}{\langle[\eta_\alpha^i(0)]^2\rangle} \tag{8}$$

where the function $\eta_\alpha^i(t)$ equals 1 if the tagged ith molecule of species α lies continuously at the surface within a $[0, t]$ interval, except during brief time spans of length τ, and zero otherwise. The consideration of values of τ different from zero relaxes the definition of surface residence by disregarding eventual fast recrossings of the bulk/surface boundaries occurring on time scales much smaller than the resulting τ^{res}. Following previous studies,[23] we set τ = 2 ps.

Results for ln $C_\alpha^{res}(t)$ for liquid-mixture/air interfaces are depicted in Figure 5. After initial, ∼2 ps, time intervals all curves can be reasonably approximated by single exponentials. Estimates for τ^{res} obtained from linear fittings of the decays for t > 5 ps appear in columns 2 and 3 of Table 2. Incidentally, we

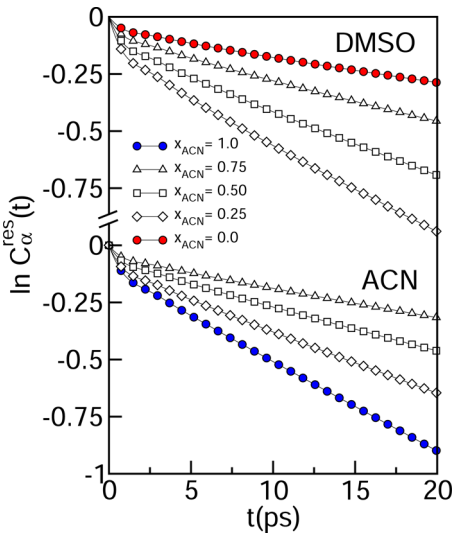

Figure 5. Population relaxations of DMSO (top curves) and ACN (bottom curves) molecules lying at liquid-mixture/air interfaces. Also shown are results for pure liquid phases (colored circles).

would like to remark that the reported value of τ_{DMSO}^{res} for pure DMSO exceeds the one reported in ref 44 by a factor of ∼2.5; we attribute this discrepancy to a deficiency of the *FS* Hamiltonian for DMSO, which also underestimates the diffusion constant in the bulk.[31] Coming back to the results listed in Table 2, two features are worth remarking: (i) residence times for both species present steady increments as the molar fraction of ACN diminishes and (ii) at fixed concentrations the values of τ_{ACN}^{res} look longer than the corresponding τ_{DMSO}^{res}. Note that while the former trend (i) is also observed in the bulk, the latter (ii) is just the opposite one, since diffusion constants for ACN in bulk mixtures are larger than those reported for DMSO.[11] The latter feature, in turn, would corroborate the more marked stabilization of ACN at the interfaces. Similar arguments have been raised to rationalize longer residence times of methanol and acetone in aqueous mixtures,[22,60] although in the latter cases, the reasons for the stabilizations were rationalized in terms of the hydrophobic-like characteristics of liquid/vapor interfaces.[24−26]

One can further explore the physical grounds underlying the latter feature by combining our previous surface/bulk equilibrium description of the slab along with the classical model by Zwanzig,[61] that portraits diffusion in the bulk as a sequence of uncorrelated activated jumps, involving passages over free energy barriers of magnitude $\Delta F^\dagger$. Let us now focus on the transfer of a tagged molecule of species α from the surface into the bulk. Assuming that the activation barrier picture still holds for this process, surface-to-bulk transfers should involve surmounting a lower free energy barrier of magnitude $\Delta F_\alpha^\dagger - \gamma_\alpha \bar{A}$. Consequently, a simple transition state theory treatment leads to the following expression for the ratio between the residence times of the two components:

$$\frac{\tau_{ACN}^{res}}{\tau_{DMSO}^{res}} \sim \exp(-\beta\Delta F) \tag{9}$$

with

$$\Delta F = \Delta F_{DMSO}^\dagger - \Delta F_{ACN}^\dagger + (\gamma_{ACN}^{lv} - \gamma_{DMSO}^{lv})\bar{A} \tag{10}$$

where we have disregarded eventual differences in the temporal prefactors that relate the exchange rates for the two species with the corresponding Boltzmann factors. By replacing estimates for $\Delta F_{DMSO}^\dagger$ = 12 kJ mol^{-1} and $\Delta F_{ACN}^\dagger$= 11 kJ mol^{-1} reported in refs 62 and 63 and the aforementioned values of the surface tensions in eqs 9 and 10, our approximated approach yields $\tau_{ACN}^{res}/\tau_{DMSO}^{res}$ = 1.4, a value that compares favorably well with the ratios obtained from the entries of Table 2, which are intermediate between 1.38 and 1.46. The previous "back-of-the-envelope" calculation involves several approximations requiring further validations; in particular, the one assuming that the magnitudes of the diffusion free energy barriers in the isotropic pure liquids environments can be directly transferred to estimate those modulating jumps along perpendicular directions in liquid-mixtures/vapor interfaces. Anyhow, the quality of the agreement might indicate that the previous hypothesis is valid or the eventual differences cancel out in the subtraction that appears in the second term of eq 10. As such, our results would indicate that Zwanzig's activation-energy picture provides a simple explanation for the differences observed in the residence times. We finally stress that our attempts to obtain meaningful information for the exchange dynamics of molecules at liquid/graphene interfaces turned out unsuccessful. At these environments, we found that τ_α^{res} values

DOI: 10.1021/acs.jpcc.7b03154
J. Phys. Chem. C 2017, 121, 14618−14627

Table 2. Dynamical Characteristics of ACN/DMSO Mixtures at Different Interfaces[a]

			liquid/air		liquid/graphene	
x_{ACN}	τ^{res}_{ACN}	τ^{res}_{DMSO}	τ^{μ}_{ACN}	τ^{μ}_{DMSO}	τ^{μ}_{ACN}	τ^{μ}_{DMSO}
0.0		88 ± 7		8.9 ± 0.5 (16.7)		
0.25	76 ± 4	55 ± 5	4.2 ± 0.2 (9.5)	7.1 ± 0.4 (14.5)	35 ± 3	46 ± 3
0.50	51 ± 5	35 ± 5	3.4 ± 0.3 (6.3)	5.5 ± 0.4 (10.6)	25 ± 3	31 ± 3
0.75	37 ± 3	26 ± 4	2.5 ± 0.3 (5.2)	4.4 ± 0.3 (8.8)	22 ± 2	28 ± 3
1.0	25 ± 3		1.9 ± 0.2 (3.5)			

[a]Times are expressed in ps. Uncertainties correspond to dispersions between results from five statistically independent trajectories lasting 10 ns each. The entries between parentheses correspond to reference results for bulk mixtures (see text).

stretch into the ns time domain, bringing the lengths of our simulations runs insufficient to harvest appropriate statistics.

The characteristics of the orientational mobilities at the interfaces were analyzed by computing individual dipole−dipole time correlation functions of the type

$$C^{\alpha}_{\mu}(t) = \frac{\langle \delta\boldsymbol{\mu}_i^{\alpha}(t)\cdot\delta\boldsymbol{\mu}_i^{\alpha}(0)\rangle_{srf}}{\langle |\delta\boldsymbol{\mu}_i^{\alpha}(0)|^2\rangle_{srf}} \quad (11)$$

where $\delta\boldsymbol{\mu}_i^{\alpha}(t) = \boldsymbol{\mu}_i^{\alpha}(t) - \langle\boldsymbol{\mu}_i^{\alpha}\rangle_{srf}$. Plots for ln C^{α}_{μ} for liquid/air interfaces are displayed in Figure 6, whereas characteristic time

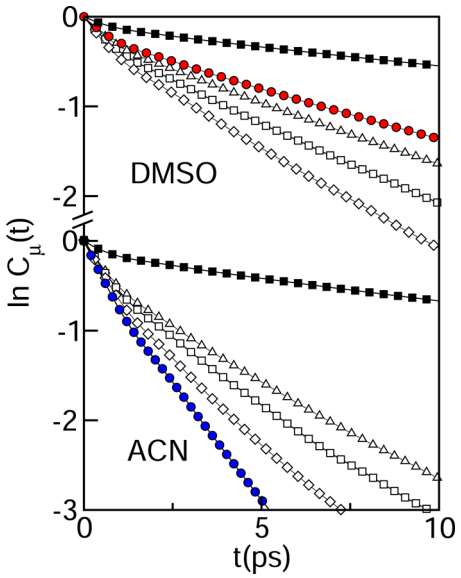

Figure 6. Orientational relaxations of DMSO (top curves) and ACN (bottom curves) molecules lying at liquid-mixture/air interfaces. Same labeling as in Figure 5. Results shown with black squares correspond to an x_{ACN} = 0.5 mixture at the liquid-mixture/graphene (Q = 0) interface.

scales for rotational motions, τ^{μ}_{α}, appear in columns 4 and 5 of Table 2. The latter values correspond to linear fits of the plots for t > 3 ps. The simultaneous inspection of the curves in Figure 6 and the entries in Table 2 reveal gradual retardations in the dynamics of both components as the concentration of ACN diminishes. This concentration trend is in agreement with the one registered for residence time scales. In this context, it is also interesting to compare values of τ^{μ}_{α} to those observed in the bulk, also listed between parentheses in the aforementioned table. In all cases, the looser structure at the surface due to the reduction in the intermolecular connectivity leads to faster decorrelations in the orientational dynamics, with characteristic times which are approximately one-half of those registered in the bulk. The entries listed in the last two columns at the right-hand side of Table 2 reveal that orientational time scales at the walls are practically 1 order of magnitude longer than those reported for liquid-mixture/air interfaces.

We will close this section by briefly commenting on the characteristics of spectral shifts in the infrared spectra of the two components at these interfaces. Signals from localized vibrations along the C−H bonds obtained from surface-selective techniques are known to be adequate to gauge the modifications operated in concentrations and intermolecular connectivities at liquid/vapor interfaces.[14,17,50,64] Within the simplest classical approach, information about IR C−H bands can be obtained from Fourier transforms of velocity time correlation functions of interfacial H-sites, namely

$$I(\omega) \propto \int_{-\infty}^{\infty} C_{vv}(t)\cos\omega t\ dt \quad (12)$$

where

$$C_{vv}(t) = \langle \mathbf{v}_i^{H}(0)\cdot\mathbf{v}_i^{H}(t)\rangle_{srf} \quad (13)$$

In Figure 7, we present results for $I(\omega)$ for the representative x_{ACN} = 0.5 mixture. In the abscissa axis, frequency shifts $\Delta\omega$ are

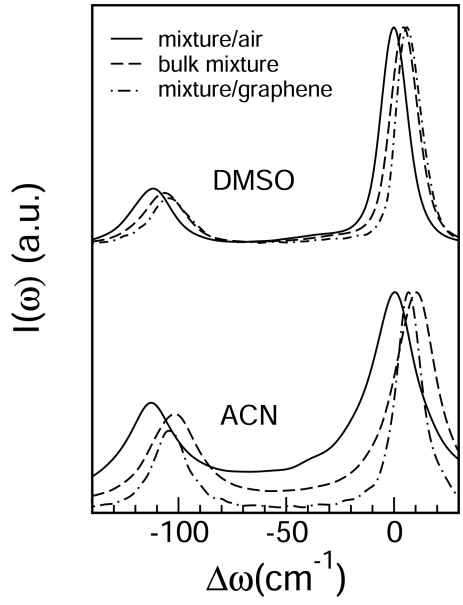

Figure 7. Infrared bands corresponding to C−H symmetric (low frequencies) and asymmetric (high frequencies) stretching modes for ACN/DMSO mixtures at different environments. The frequency shifts are expressed relative to the position of the asymmetric band in mixture/air interfaces. To facilitate the comparison, the heights of the asymmetric bands were brought to a same value.

DOI: 10.1021/acs.jpcc.7b03154
J. Phys. Chem. C 2017, 121, 14618−14627

expressed relative to the positions of the centers of the corresponding asymmetric stretch bands for liquid/air interfaces. In passing, we remark that we made no efforts to modify the parametrization of our intramolecular Hamiltonians to bring the positions of the different bands in agreement with experimental information. As such, our force field predicts C−H peaks that fall, typically, ∼100 cm^{-1} blue-shifted. All plots shown in Figure 7 present two bands, which we assign to symmetric (low frequencies) and asymmetric (high frequencies) C−H modes. Moreover, the signals for the bulk (dashed lines) appear ∼10 cm^{-1} blue-shifted with respect to the liquid/air interfaces (solid lines). This trend has been previously reported by Allen et al.,[14,17] who performed vibrational sum frequency spectroscopic experiments liquid/air interfaces involving water/DMSO mixtures. Note that this peculiar behavior is at odds with the one observed in interfaces involving strong hydrogen-bonded substances, like water/vapor ones, in which the presence of dangling hydrogens shift surface frequencies toward higher frequencies, compared to the bulk ones. Contrasting, here, the intermolecular connectivity involving CH_3 groups would be compatible with what is usually referred to as X−H···Y, "improper hydrogen bonds". The latter terminology that has been coined to denote coordination-induced, X−H bond contractions.[65,66] In fact, results from quantum calculations indicate that the resulting modifications of the X−H distances are the result of charge transfer processes controlled by a competition between, on the one hand, the electron affinity of the donor-atom X and, on the other, the attractive interaction between the positively charged H and the acceptor-atom Y. Surprisingly enough, despite the simplicity of the our classical force field, our simulation result predict not only the observed blue-shift trend in the bulk but also the correct order of magnitude, i.e., ∼10−20 wavenumbers. We remark that we found no relevant modifications in the C−H bond lengths between bulk and surface molecules to corroborate this way of reasoning. However, this should not be totally unexpected, considering that electronic structure calculations show that modifications in the X−Y distance of the order of 10^{-2} Å are enough to explain the frequency shifts. Finally, note that as a result of additional wall−CH_3 interactions, the signals corresponding to liquid/graphene interfaces practically coincide with the bulk ones.

V. CONCLUDING REMARKS

We have presented a detailed analysis that included structural characteristics and key dynamical properties of aprotic mixtures combining ACN and DMSO at different interfaces. At liquid/vapor ones, our simulations reveal a clear preference of ACN to lie adjacent to the vapor phase. For example, for x_{ACN} = 0.25 mixtures, deviations in the local concentrations from the bulk-mixture values are reflected in practically ∼70% increments in the ACN surface density. By considering a simple model in which interfacial and bulk environments are pictured as two phases in equilibrium, we succeeded in describing the extent of this tendency remarkably well. Moreover, the implemented model clearly indicates that the sole consideration of the difference between the air/liquid surface tensions of the pure liquids would be enough to reproduce the simulation results.

The analysis of orientational correlations was evaluated in terms of distributions of the individual dipolar alignments with respect to the direction normal to the liquid/vapor interfaces. Starting from ACN-rich solutions, we observed a mild tendency toward orientations in which the dipoles point out, into the gas phase; contrasting, in DMSO-rich scenarios, the preferential orientations look mostly parallel to the interface. The incorporation of wall/solvent dispersive forces that prevail close to hydrophobic-like solid plates leads to stronger restrictions in orientational fluctuations of the adjacent liquid phases. For equimolar mixtures, the vast majority of the ACN molecules present dipolar alignments parallel to the plates, along with a much minor fraction, that expose the distal methyl group to the solid phase. The complex interplay between the variety of distances describing the geometry of DMSO molecules along with those describing the individual site−wall interactions precluded a clear interpretation of the local solvation structure of the latter component. Still, the dipolar distribution for DMSO presents a much more simple bimodal character, suggesting local arrangements, with equally likely parallel and antiparallel alignments.

Contrasting with the liquid/vapor interface description, the previously reported ACN surface propensity reverses at hydrophobic walls, giving rise to somewhat less marked, albeit clear, enhancements of DMSO concentrations. Interestingly, a similar equilibrium analysis, expressed now in terms of differences in the corresponding solid/liquid surface tensions was also found to be adequate to explain the inversion in the competition for interfacial positions. The incorporation of Coulomb coupling between the graphene walls and the liquid phase, in turn, reinforced the DMSO propensity most notably, close to the cathode wall. As expected, this additional coupling modified the orientational distributions toward profiles which were accordant with the presence of a net polarization across the fluid phase, parallel to the external electric field. The preferential solvation of DMSO at charged plates observed here would agree with magnitudes of the signals of interfacial infrared spectroscopy measurements reported in ref 67.

The concentration dependence of the overall dynamics of the mixtures at the interfaces followed trends similar to the ones observed in the bulk. As such, the characteristic time scales describing the different dynamical modes stretched, as the concentration of ACN diminished. As a singularity, at fixed concentrations, we detected ACN residence times at liquid/vapor interfaces longer than those observed for DMSO molecules, despite the fact that in the bulk, ACN molecules diffuse faster than DMSO ones. By combining the bulk-interface equilibrium description with the activated picture of diffusion proposed by Zwanzig, we succeeded in interpreting the latter differences invoking classical transition state theory arguments. Still, the transferability of estimates for free energy barriers controlling isotropic diffusive motions in the bulk to those modulating anisotropic modes at interfaces deserves further investigations which are well beyond the scope of this work.

Finally, we performed a classical analysis to detect spectral shifts in the IR spectra of surface molecules by focusing on the corresponding C−H stretching bands. Despite the simplicity of our Hamiltonian, we found spectral shifts that agree at a qualitative level with those reported from surface-sensitive spectroscopic techniques. These modifications are compatible with the presence of "blue-shifted" hydrogen bonds, contrasting sharply with the red-shifts otherwise recorded in interfacial scenarios hosting strongly hydrogen-bonded substances.

Summarizing, the simulation results presented in this paper shed light on a variety of new behaviors that complement previous studies dealing with mixtures combining, for example, protic/aprotic components at different interfaces. Our

DOI: 10.1021/acs.jpcc.7b03154
J. Phys. Chem. C 2017, 121, 14618−14627

description is far from complete and further analyses will be necessary to bring additional support to several of the approximations underlying the main conclusions drawn from this study. Yet, our physical interpretations, based on fundamental physicochemical arguments, would confirm that our approach retains the key ingredients controlling the structure and the dynamical behavior of aprotic mixtures at liquid/air and liquid/graphene interfaces.

AUTHOR INFORMATION

Corresponding Author

*E-mail dhlaria@cnea.gov.ar; Ph +54 (11)67727048; Fax +54 (11)67727121.

ORCID

Daniel Laria: 0000-0002-4457-6269

Notes

The authors declare no competing financial interest.

ACKNOWLEDGMENTS

J.R., M.D.E., and D.L. are staff members of CONICET-Argentina and acknowledge the support of this research from CONICET (PIP 112-20110100464). J.M. acknowledges financial support from the Ministerio de Economía y Competitividad de España (Proyecto FIS2015-66879-C2-1-P).

REFERENCES

(1) McGann, L. E.; Walterson, M. L. Cryoprotection by Dimethyl Sulfoxide and Dimethyl Sulfone. *Cryobiology* **1987**, *24*, 11−16.

(2) Dorsey, J. G.; Dill, K. A. The Molecular Mechanism of Retention in Reversed-Phase Liquid Chromatography. *Chem. Rev.* **1989**, *89*, 331−346.

(3) Huggins, R. *Energy Storage: Fundamentals, Materials and Applications*; Springer: New York, 2015.

(4) David, N. A. The Pharmacology of Dimethyl Sulfoxide. *Annu. Rev. Pharmacol.* **1972**, *12*, 353−374.

(5) de Gouw, J. A.; Warneke, C.; Parrish, D. D.; Holloway, J. S.; Trainer, M.; Fehsenfeld, F. C. Emission Sources and Ocean Uptake of Acetonitrile (CH_3CH) in the Atmosphere. *J. Geophys. Res.* **2003**, *108*, ACH 2-1−ACH 2-8.

(6) Cooke, C.; McCallum, C.; Pethybridge, A. S.; Prue, J. E. Conductance of Acids in Dimethylsulfoxide-I. Conductance of Hydrochloric Acid in DMSO-Water Mixtures at 25°C. *Electrochim. Acta* **1975**, *20*, 591−598.

(7) Kolthoff, I. M.; Bruckenstein, S.; Chantooni, M. K., Jr. Acid-Base Equilibria in Acetonitrile. Spectrophotometric and Conductometric Determination of the Dissociation of Various Acids. *J. Am. Chem. Soc.* **1961**, *83*, 3927−3935.

(8) Laria, D.; Kapral, R.; Estrin, D.; Ciccotti, G. Molecular Dynamics Study of Solvation Effects on Acid Dissociation in Aprotic Media. *J. Chem. Phys.* **1996**, *104*, 6560−6568.

(9) Semino, R.; Zaldívar, G.; Calvo, E. J.; Laria, D. Lithium Solvation in Dimethyl Sulfoxide Acetonitrile Mixtures. *J. Chem. Phys.* **2014**, *141*, 214509.

(10) Mozhzhukhina, N.; Longinotti, M. P.; Corti, H.; Calvo, E. J. A Conductivity Study of Preferential Solvation of Lithium Ion in Acetonitrile-Dimethyl Sulfoxide Mixtures. *Electrochim. Acta* **2015**, *154*, 456−461.

(11) Bernardi, E.; Stassen, H. Molecular Dynamics Simulations of Acentonitrile/Dimethylsulfoxide Liquid Mixtures. *J. Chem. Phys.* **2004**, *120*, 4860−4867.

(12) Fort, J.; Moore, W. R. Adiabatic Compressibilities of Binary Liquid Mixtures. *Trans. Faraday Soc.* **1965**, *61*, 2102−2111.

(13) Mountain, R. D. Molecular Dynamics Simulation of Water-Acetonitrile Mixtures in a Silica Slit. *J. Phys. Chem. C* **2013**, *117*, 3923−3929.

(14) Allen, H. C.; Raymond, E. A.; Richmond, G. L. Non-Linear Vibrational Sum Frequency Spectroscopy of Atmospherically Relevant Molecules at Aqueous Solution Surfaces. *Curr. Opin. Colloid Interface Sci.* **2000**, *5*, 74−80.

(15) Makowski, M. J.; Stern, A. C.; Hemminger, J. C.; Tobias, D. J. Orientation and Structure of Acetonitrile in Water at the Liquid-Vapor Interface: A Molecular Dynamics Simulation Study. *J. Phys. Chem. C* **2016**, *120*, 17555−17563.

(16) Zhang, D.; Gutow, J. H.; Eisenthal, K. B.; Heinz, T. F. Sudden Structural Change at the Air/Binary Liquid Interface: Sum Frequency Study of the Air/Acentonitrile Interface. *J. Chem. Phys.* **1993**, *98*, 5099−5101.

(17) Allen, H. C.; Gragson, D. E.; Richmond, G. L. Molecular Structure and Adsorption of Dimethyl Sulfoxide at the Surface of Aqueous solutions. *J. Phys. Chem. B* **1999**, *103*, 660−666.

(18) Fábián, B.; Idrissi, A.; Marekha, B.; Jedlovszky, P. Local Lateral Environment of the Molecules at the Surface of DMSO-Water Mixtures. *J. Phys.: Condens. Matter* **2016**, *28*, 404002.

(19) Rivera, C. A.; Bender, J. S.; Manfred, K.; Fourkas, J. T. Persistence of Acetonitrile Bilayers at the Interface Acetonitrile/Water Mixtures with Silica. *J. Phys. Chem. A* **2013**, *117*, 12060−12066.

(20) Idrissi, A.; Marekha, B.; Kiselev, M.; Jedlovszky, P. The Local Environment of Molecules in Water-DMSO Mixtures, as seen from Computer Simulations and Voronoi Polyhedra Analysis. *Phys. Chem. Chem. Phys.* **2015**, *17*, 3470−3481.

(21) Mountain, R. D. Microsctructure and Hydrogen Bonding in Water-Acetonitrile Mixtures. *J. Phys. Chem. B* **2010**, *114*, 16460−16464.

(22) Fábián, B.; Jójárt, B.; Horvai, G.; Jedlovszky, P. Properties of the Liquid-Vapor Interface of Acetone-Water Mixtures. A Computer Simulation and ITIM Analysis Study. *J. Phys. Chem. C* **2015**, *119*, 12473−12487.

(23) Pártay, L. B.; Jedlovszky, P.; Horvai, G. Structure of the Liquid-Vapor Interface of Water-Acetonitrile Mixtures as seen from Molecular Dynamics Simulations and Identification of Truly Interfacial Molecules Analysis. *J. Phys. Chem. C* **2009**, *113*, 18173−18183.

(24) Bresme, F.; Chacón, P.; Tarazona; Tay, K. Intrinsic Structure of Hydrophonic Surfaces: The Oil-Water Interface. *Phys. Rev. Lett.* **2008**, *101*, 056102.

(25) Remsing, R. C.; Rodgers, J. M.; Weeks, J. D. Deconstruction Classical Water Models at Interfaces and in Bulk. *J. Stat. Phys.* **2011**, *145*, 313−334.

(26) Willard, A. P.; Chandler, D. The Molecular Structure of the Interface between Water and a Hydrophobic Substrate is Liquid-Vapor Like. *J. Chem. Phys.* **2014**, *141*, 18C519.

(27) Rodriguez, J.; Elola, M. D.; Laria, D. Coaxial Cross-Diffusion through Carbon Nanotubes. *J. Phys. Chem. B* **2009**, *113*, 14844−14848.

(28) Grande, L.; Paillard, E.; Hassoun, J.; Park, J.-B.; Lee, Y.-J.; Sun, Y.-K.; Passerini, S.; Scrosati, B. The Lithium/Air Battery: Still an Emerging System or a Practical Reality? *Adv. Mater.* **2015**, *27*, 784−800.

(29) Nosé, S. Unified Formulation of the Constant Temperature Molecular-Dynamics Methods. *J. Chem. Phys.* **1984**, *81*, 511−519.

(30) Hoover, W. G. Canonical Dynamics: Equilibrium Phase-Space Distributions. *Phys. Rev. A: At., Mol., Opt. Phys.* **1985**, *31*, 1695−1697.

(31) Strader, M.; Feller, S. E. Flexible All-Atom Model of Dimethyl Sulfoxide for Molecular Dynamics Simulations. *J. Phys. Chem. A* **2002**, *106*, 1074−1080.

(32) Nikitin, A. M.; Lyubartsev, A. P. New Six-site Acetonitrile Model for Simulations of Liquid Acetonitrile and its Aqueous Mixtures. *J. Comput. Chem.* **2007**, *28*, 2020−2026.

(33) Phillips, C.; Braun, R.; Wang, W.; Gumbart, J.; Tajkhorshid, E.; Villa, E.; Chipot, C.; Skeel, R. D.; Kale, L.; Schulten, K. Scalable Molecular Dynamics with NAMD. *J. Comput. Chem.* **2005**, *26*, 1781−1802.

(34) Foloppe, N.; Mac Kerrell, A. D., Jr. All-Atom Empirical Force Field for Nucleic Acids: I. Parameter Optimization Based on Small

DOI: 10.1021/acs.jpcc.7b03154
J. Phys. Chem. C 2017, 121, 14618−14627

Molecule and Condesed Phase Macromolecular Target Data. *J. Comput. Chem.* **2000**, *21*, 86−104.
(35) Merlet, C.; Péan, C.; Rotenberg, P. A.; Simon, B.; Madden, P.; Salanne, M. Simulating Supercapacitors: Can We Model Electrodes as Constant Charge Surfaces? *J. Phys. Chem. Lett.* **2013**, *4*, 264−268.
(36) Siepmann, J. I.; Sprik, M. Influence of Surface Topology and Electrostatic Potential on Water/Electrode Systems. *J. Chem. Phys.* **1995**, *102*, 511−524.
(37) Wang, Z.; Yang, Y.; Olmsted, D. L.; Asta, M.; Laird, B. B. Evaluation of the Constant Potential Method in Simulating Electric Double-Layer Capacitors. *J. Chem. Phys.* **2014**, *141*, 184102.
(38) Chacón, E.; Tarazona, P. Intrinsic Profiles beyond the Capillary Wave Theory: A Monte Carlo Study. *Phys. Rev. Lett.* **2003**, *91*, 166103.
(39) Chacón, E.; Tarazona, P.; Alejandre, J. The Intrinsic Structure of the Water Surface. *J. Chem. Phys.* **2006**, *125*, 014709.
(40) Fern, J. R.; Keffer, D. J.; Steele, W. V. Vapor-Liquid Equilibrium of Ethanol by Molecular Dyanamics Simulation and Voronoi Tesselation. *J. Phys. Chem. B* **2007**, *111*, 13278−13286.
(41) Willard, A.; Chandler, D. Instantaneous Liquid Interfaces. *J. Phys. Chem. B* **2010**, *114*, 1954−1958.
(42) Jorge, M.; Jedlovszky, P.; Cordeiro, M. N. D. S. A Critical Assessment of Methods for the Intrisic Analysis of Liquid Interface. 1. Surface Site Distributions. *J. Phys. Chem. C* **2010**, *114*, 11169−11179.
(43) Pártay, L. B.; Hantal, G.; Jedlovszky, P.; Vincze, A.; Horvai, G. A New Method for Determining the Interfacia Molecules and Characterizing the Surface Roughness in Computer Simulations. Applications to the Liquid-Vapor Interface of Water. *J. Comput. Chem.* **2008**, *29*, 945−956.
(44) Darvas, M.; Jojják, K.; Horvai, G.; Jedlovszky, P. Molecular Dynamics Simulation and Identification of the Truly Interfacial Molecules (ITIM) Analysis of the Liquid-Vapor Interface of Dimethylsulfoxide. *J. Chem. Phys.* **2010**, *132*, 134701.
(45) Butler, J. A. V. The Thermodynamics of the Surfaces of Solutions. *Proc. R. Soc. London, Ser. A* **1932**, *135*, 348−375.
(46) Nath, S. Surface Tension of Nonideal Binary Liquid Mixtures as a Function of Composition. *J. Colloid Interface Sci.* **1999**, *209*, 116−122.
(47) Jasper, J. J. The Surface Tension of Pure Liquid Compounds. *J. Phys. Chem. Ref. Data* **2009**, *1*, 841−1010.
(48) Paul, S.; Chandra, A. Molecular Dynamics Study of th Liquid-Vapor Interface of Acetonitrile: Equilibrium and Dynamical Properties. *J. Phys. Chem. B* **2005**, *109*, 20558−20564.
(49) Hu, Z.; Weeks, J. D. Acetonitrile on Silica Surfaces and at Its Liquid-Vapor Interface: Structural Correlations and Collective Dynamics. *J. Phys. Chem. C* **2010**, *114*, 10202−10211.
(50) Velarde, L.; Zhang, X.-y.; Lu, Z.; Joly, A. G.; Wang, Z.; Wang, H.-f Communication: Spectroscopic Phase and Lineshapes in High-Resolution Broadband Sum Frequency Vibrational Spectroscopy: Resolving Interfacial Inhomogeneities of "Identical" Molecular Groups. *J. Chem. Phys.* **2011**, *135*, 241102.
(51) Shen, J.; He, Y.; Wu, J.; Gao, C.; Zhang, X.; Yang, Y.; Ye, M.; Vajtai, R.; Lou, J.; Ajayan, P. M.; et al. Liquid Phase Exfoliation of Two-Dimensional Materials by Directly Probing and Matching Surface Tension Components. *Nano Lett.* **2015**, *15*, 5449−5454.
(52) Owens, D. K. Some Thermodynamic Aspects of Polymer Adhesion. *J. Appl. Polym. Sci.* **1970**, *14*, 1725−1730.
(53) Fowkes, F. M. Attractive Forces at Interfaces. *Ind. Eng. Chem.* **1964**, *56*, 40−52.
(54) See Table S1 in the Supporting Information for ref 51.
(55) Meyer, M.; Mareschal, M.; Hayoun, M. A Comparison of the Structure and Dynamics of Liquid Water at Hydrophobic and Hydrophilic Surfaces - A Molecular Dyanmics Simulation Study. *J. Chem. Phys.* **1988**, *89*, 1067−1073.
(56) Michael, D.; Benjamin, I. Molecular Dynamics Simulation of the Water|Nitrobenzene Interface. *J. Electroanal. Chem.* **1998**, *450*, 335−345.
(57) Benjamin, I. Theoretical Study of the Water/1,2-Dichloroethane Interface: Structure, Dynamics, and Conformational Equilibria at the Liquid-Liquid Interface. *J. Chem. Phys.* **1992**, *97*, 1432−1445.
(58) Senapati, S. A Molecular Dyanamics Simulation Study of the Dimethyl Sulfoxide Liquid-Vapor Interface. *J. Chem. Phys.* **2002**, *117*, 1812−1816.
(59) Liu, P.; Harder, E.; Berne, B. J. On the Calculation of Diffusion Coefficients in Confined Fluids and Interfaces with an Application to the Liquid-Vapor Interface of Water. *J. Phys. Chem. B* **2004**, *108*, 6595−6602.
(60) Pártay, L. B.; Jedlovszky, P.; Vincze, A.; Horvai, G. Properties of Free Surface of Water-Methanol Mixtures. Analysis of the Truly Interfacial Molecular Layer in Computer Simulation. *J. Phys. Chem. B* **2008**, *112*, 5428−5438.
(61) Zwanzig, R. On the Relationa between Self-Diffusion and Viscosity of Liquids. *J. Chem. Phys.* **1983**, *79*, 4507−4508.
(62) Saha, N.; Das, B.; Hazra, D. K. Viscosities and Excess Molar Volumes for Acetonitrile + Methanol at 298.15, 308.15, and 318.15 K. *J. Chem. Eng. Data* **1995**, *40*, 1264−1266.
(63) Blokkdal, E. H. Self-Diffusion Coefficient of Bulk Fluid Molecules Probed by Transverse Relaxation Measurements in an Inhomogeneous Magnetic Field. Ms. Sci. Dissertation, University of Oslo, Norway, 2014.
(64) Lu, R.; Gan, W.; Wu, B.-h.; Zhang, Z.; Guo, Y.; Wang, H.-f. C-H Stretching Vibrations of Methyl, Methylene and Methine Groups at the Vapor/Alcohol (n = 1−8) Interfaces. *J. Phys. Chem. B* **2005**, *109*, 14118−14129.
(65) Joseph, J.; Jemmis, E. D. Red-, Blue-, or No-Shift in Hydrogen Bonds: a Unified Explanation. *J. Am. Chem. Soc.* **2007**, *129*, 4620−4632.
(66) Li, X.; Liu, L.; Schlegel, H. B. On the Physical Origin of Blue-Shifted Hydrogen Bonds. *J. Am. Chem. Soc.* **2002**, *124*, 9639−9647.
(67) Roelfs, B.; Schröter, C.; Solomun, T. A. Comparison of Metal/Vaccum and Metal/Electrolyte Interfaces: The Au(100)/(Dimethylsulfoxide) and (Dimethylsulfoxide+Acetonitrile) Systems. *Ber. Bunsen-Ges. Phys. Chem.* **1997**, *101*, 1105−1112.

DOI: 10.1021/acs.jpcc.7b03154
J. Phys. Chem. C 2017, 121, 14618−14627